

RESEARCH

Open Access



Taurultam shows antiviral activity against SARS-CoV-2 and influenza virus

Rongbo Luo^{1†}, Beilei Shen^{1†}, Bingshuo Qian^{1,2†}, Lingjun Fan^{1,3}, Junkui Zhang^{1,2}, Xiuwen Deng^{1,4}, Yan Sun^{1,5}, Shijun Zhang^{1,4}, Tiecheng Wang^{1,6}, Yuanguo Li¹, Weiyang Sun^{1,6}, Xiaobin Pang^{2*}, Wu Zhong^{7*} and Yuwei Gao^{1,2,3,4,5,6*}

Abstract

Background SARS-CoV-2 and influenza virus are highly contagious respiratory viruses that continuously pose major threats to human and public health. The high frequency of viral mutations led to the emergence of resistant isolates and caused virus epidemics repeatedly, emphasizing the urgent need to develop new antivirals. Taurultam is a metabolite of taurolidine. Moreover, taurolidine has been shown to have potent antiviral activities against multiple viruses and to have antiviral effects through its metabolites.

Results In this study, we sought to determine the antiviral activities of taurultam against SARS-CoV-2 and influenza virus in Vero-E6, Huh7, 293T-ACE2, and MDCK cell lines and mouse infection models. The results showed that taurultam exhibited potent antiviral activity against multiple SARS-CoV-2 variants, influenza A (H1N1, H3N2) virus and influenza B virus, in vitro. Moreover, in influenza A (H1N1) virus, influenza B virus and SARS-CoV-2 infection models, taurultam significantly reduced viral loads, increased survival, improved mouse body weight and lung injury. Surprisingly, taurultam treatment not only inhibited the influenza A virus and SARS-CoV-2, but also benefited for therapy of mixed infection of these two viruses in vitro, demonstrating the great antiviral potential of taurultam for the treatment of SARS-CoV-2 and influenza virus infections.

Conclusions Together, our findings identify taurultam as a new candidate for the treatment of SARS-CoV-2 and influenza virus infections, especially virus-induced lung pathology.

Clinical trial number Not applicable.

Keywords SARS-CoV-2, Influenza virus, Antiviral, Lung injury, Taurultam, Taurolidine metabolite

[†]Rongbo Luo, Beilei Shen and Bingshuo Qian contributed equally to this work.

*Correspondence:

Xiaobin Pang
pxb@vip.henu.edu.cn

Wu Zhong
zhongwu@bmi.ac.cn

Yuwei Gao
dawei1105@foxmail.com

¹Changchun Veterinary Research Institute, State Key Laboratory of Pathogen and Biosecurity, Key Laboratory of Jilin Province for Zoonosis Prevention and Control, Chinese Academy of Agricultural Sciences, Changchun 130122, China

²School of Pharmacy, Henan University, Kaifeng 475004, China

³Engineering Research Center of Glycoconjugates, Ministry of Education, Jilin Provincial Key Laboratory of Chemistry and Biology of Changbai Mountain Natural Drugs, School of Life Sciences, Northeast Normal University, Changchun 130024, China

⁴College of Integrated Chinese and Western Medicine, Changchun University of Chinese Medicine, Changchun, Jilin 130117, China

⁵College of Veterinary Medicine, Shanxi Agricultural University, Jinzhong 030801, China

⁶Jiangsu Co-innovation Center for Prevention and Control of Important Animal Infectious Diseases and Zoonoses, Yangzhou University, Yangzhou 225009, PR China

⁷National Engineering Research Center for the Emergency Drug, Beijing Institute of Pharmacology and Toxicology, Beijing 100850, China



Background

The COVID-19 outbreak, caused by SARS-CoV-2, has led to a global health crisis and a rapid wave of antiviral drug research and development. Following virus variation and strong prevention and control measures, the threat from new SARS-CoV-2 strains has decreased [1]. Although long-term hygiene and physical distancing measures have prevented the spread of SARS-CoV-2 and other viruses, the decrease in human-specific immunity has led to rapid sweeping of other respiratory viruses across the world, such as influenza viruses, which cause high morbidity and mortality in winter [2, 3]. In addition, as the virus accumulates novel mutations, novel variants with resistance mutations may reduce the efficacy of existing antiviral drugs [4] and highlight more effective antiviral strategies, especially the development of broad-spectrum antivirals according to conserved pathogenic mechanisms.

Taurolidine [5], which has antimicrobial and anti-inflammatory properties, was originally used in peritonitis and catheter-related blood stream infections [6–8] and was proven to have broad-spectrum antiviral activities against highly pathogenic influenza A (H5N1) virus and SARS-CoV-2 [9]. From pharmacokinetics studies, we found that taurolidine has a short half-life in vivo and is metabolized to taurultam and taurinamide [10]. To determine whether taurolidine metabolites also have antiviral activities, taurultam was investigated in this study. In vitro results revealed that taurultam exhibited potent antiviral activity against multiple SARS-CoV-2 variants, influenza A (H1N1, H3N2) virus and influenza B virus (IBV). Alternatively, taurultam treatment not only inhibited the influenza A virus and SARS-CoV-2 alone, but also benefited for therapy of mixed infection of these two viruses, demonstrating the great antiviral potential of taurultam for SARS-CoV-2 and influenza viruses.

Materials and methods

Cell lines and animals

The following cell lines were used in this study: Africa green monkey cells (Vero-E6), human hepatocarcinoma cell line (Huh7), Madin-Darby canine kidney (MDCK), and human embryonic kidney cell line (293T-ACE2) from the Chinese Academy of Agricultural Sciences. All the cell lines were cultured in complete Dulbecco's modified Eagle's medium (DMEM, Corning, Cat. #10–013-CVRC) supplemented with 10% FBS (Gibco, Cat. #A5669801), 100 IU/mL penicillin and 100 mg/mL streptomycin (Gibco, Cat. #15140122). Female BALB/c mice, C57BL/6 N mice (8–9 months old) and golden hamsters (4 weeks old) were purchased from Beijing Vital River Laboratory Animal Technology Co., Ltd. (Beijing, China). All animal experiments were performed according to the

regulations and bioethics guidelines (approval number: IACUC of AMMS-11-2022-036).

Viruses

All SARS-CoV-2 isolates used in this study were preserved in the biosafety level 3 laboratory of the Changchun Veterinary Research Institute, Chinese Academy of Agricultural Sciences (CAAS) and were propagated and titrated by TCID₅₀ in Vero-E6 cells before use. SARS-CoV-2/C57MA14, a mouse adapted strain, was derived from SARS-CoV-2/BJ01 by serial passaging in C57BL/6 N mice and was preserved as other SARS-CoV-2 isolates. The H1N1/UI182 strain, influenza B virus IBV/S9-E2 strain and IBV/S9-MD strain were stored as previously described [11]. The H3N2 strain was also isolated by the Changchun Veterinary Research Institute. All the influenza A virus strains were propagated and titrated by the EID₅₀ in 11–12-day-old chicken embryos at 37 °C and influenza B virus strains were propagated and titrated by EID₅₀ in 9–10-day-old chicken embryos at 33 °C. All viruses were maintained and used according to biosafety regulations.

Drug Preparation

Taurultam and molnupiravir (also named EIDD-2801 or MK-4482, has been used clinically for COVID-19 as a preferred antiviral) were gifts from Prof. Wu Zhong (National Engineering Research Center for the Emergency Drug, Beijing, China) and were dissolved in phosphate buffered saline (PBS, pH 7.4) or DMEM supplemented with 2% FBS before use. If the dissolution of molnupiravir was incomplete, a 56 °C thermal bath was used. Oseltamivir (OSTA) phosphate (for animal experiments) and oseltamivir acid (for in vitro experiments) were purchased from MCE and were dissolved in PBS.

Drug toxicity and antiviral assay

The drug toxicity and antiviral activity of taurultam were measured in the Vero-E6 cell line via a CCK-8 assay. Specifically, when the cell confluence reached 70–80%, the cells were washed with PBS and incubated with drug dilutions at the corresponding concentrations or with virus dilutions at the indicated multiplicities of infection (MOI). For the drug toxicity assay, the cells were incubated with drugs for 48 h continuously, and the cell viability was tested. For the in vitro antiviral assay, the virus dilution was discarded after incubation for 1 h, and the cells were washed with PBS. Then, the cell culture medium or drug dilution was added. At 48 h post infection (hpi), cell viability was tested, and the inhibition rate of each drug concentration was calculated. The cytotoxic concentration for 50% of the cells (CC₅₀) and the half-maximal effective concentration (EC₅₀) were automatically calculated via curve fitting.

Viral load determination

Two hundred microlitres of cell supernatants or supernatants from the lysed tissues were harvested for RNA extraction (TIANGEN, Cat. #YDP804-T1). The viral load of SARS-CoV-2 was detected by qRT-PCR assays according to the instructions of the Novel Coronavirus (2019) Nucleic Acid Detection Kit (BioPerfectus, China), which targets the SARS-CoV-2 *ORF1ab* and *N* genes. The viral load of influenza A virus was detected via a One Step RT-PCR Kit (Takara, China) targeting the *M* gene. The primers used were as follows:

SARS-CoV-2 *ORF1ab* gene:

Forward sequence: CCCTGTGGGTTTTACTACTTAA.

Reverse sequence: ACGATTGTGCATCAGCTGA.

Probe sequence: 5'-FAM-CCGTCTGCGGTATGTGGA AAGGTTATGG-BHQ1-3'.

SARS-CoV-2 *N* gene:

Forward sequence: GGGGAACTTCTCCTGCTAGAAT.

Reverse sequence: CAGACATTTTGCTCTCAAGCTG.

The probe sequence used was 5'-FAM-TTGCTGCTGCT TGACAGATT-TAMRA-3'.

H1N1M gene:

Forward sequence: 5'-GTCTTCTAACCAGGTCGAA A-3'.

Reverse sequence: 5'-AAGATCTGTGTTCTTTTCTGC AAA-3'.

Probe sequence: 5'-FAM-CCCTCAAAGCCGAGATCG C-TAMRA-3'.

Immunofluorescence assay

After virus infection, the cells were washed three times with PBS, fixed with 4% paraformaldehyde (Servicebio, Cat. #G1101) for 20 min and infiltrated with 0.2% Triton-X100 (Sigma, Cat. #T8787) for 20 min at room temperature (RT). Then, the cells were blocked with 2% BSA buffer for 1 h and incubated with primary antibody (anti-IAV nucleoprotein, Abcam, Cat. #ab128193, 1:200; anti-IBV nucleoprotein, GeneTex, Cat. #GTX128538, 1:500; anti-SARS-CoV-2 nucleoprotein, CST, Cat. #33717, 1:500) for 4 h or overnight at 4 °C. After the addition of the primary antibody, the secondary antibody (Goat Anti-Rabbit IgG H&L (Alexa Fluor® 488), Abcam, Cat. #ab150077, 1:500; Alexa Fluor® 488 AffiniPure™ Goat Anti-Mouse IgG (H + L), Jackson ImmunoResearch Laboratories, Inc, Cat. #AB_2338840, 1:500) was added, and the samples were incubated for 2 h in the dark. Finally, the nuclei were stained with DAPI (ThermoFisher, Cat. #62248, 1 µg/mL) for 10 min, and fluorescence was observed under a fluorescence microscope. After each incubation, the cells were washed with PBS three times.

In vivo experiments involving one virus infection

Female BALB/c mice, C57BL/6 N mice (8–9 months old) and 4-week-old female golden hamsters were used for

SARS-CoV-2 infection. Eight-week-old female BALB/c mice were used for influenza virus infection. After one week of adaptive feeding, the mice were randomly divided into an uninfected group (control), a virus-infected group, a taurultam-treated group, and a molnupiravir- or OSTA-treated group. The mice in each group, except those in the uninfected group, were challenged with 50 µL of virus dilution (2000 PFU of SARS-CoV-2/C57MA14; 10 × LD₅₀ influenza virus) via the nasal drop method, and the golden hamsters were challenged with 100 µL of virus dilution (10000 PFU of the BA.2 strain). The control group and virus-infected groups were treated with PBS (100 µL/mouse, and 350 µL/hamster) by intraperitoneal injection (i.p.). The taurultam treatment (200 mg/kg/day for mice, and 140 mg/kg/day for hamsters, i.p.), molnupiravir treatment (500 mg/kg/day for mice, and 350 mg/kg/day for hamsters, p.o.) or OSTA treatment (12.5 mg/kg/day for mice, p.o.) started 12 h post infection and continued until the fifth day. At 3 dpi or 5 dpi, the mice from each group were selected randomly and sacrificed for detection of the viral load in the lungs and turbinates and the severity of lung injury. The residual mice were used for body weight tests and survival analysis.

Mixed infection studies in mouse models

Coinfection with SARS-CoV-2 and influenza A (H1N1) virus was performed in 8–9 months old female BALB/c mice or 4-week-old female golden hamsters. After adaptive feeding, each mouse was challenged with 50 µL of virus dilution (1000 PFU H1N1-UI182 and 2000 PFU SARS-CoV-2/C57MA14), and each hamster was challenged with 100 µL of virus dilution (1000 PFU H1N1-UI182 and 1000 PFU Omicron BE.7) sequentially. At 12 h post infection with SARS-CoV-2, taurultam was administered via the i.p. route (200 mg/kg/day for mice, and 140 mg/kg/day for hamsters). As a control, the virus-infected group was administered PBS (100 µL/mouse, and 350 µL/hamster). At 2 dpi and 4 dpi, the mice were sacrificed, and the tissues were collected for viral load assays and histopathological analysis, while the remaining mice were maintained for body weight until 14 dpi.

Statistical analysis

All the statistical analyses were performed via GraphPad Prism 8.0.2 (GraphPad Software, USA). One-way ANOVA or Student's *t* test was used to determine significant differences. The error bars, which indicate either SEM, are mentioned in the respective figure legends. In all cases, $n \geq 3$ (special data are shown in the individual experimental group), a p value < 0.05 was considered significant, and $*P < 0.05$, $**P < 0.01$, and $***P < 0.001$.

Results

Taurultam shows potent antiviral activity against different SARS-CoV-2 variants in vitro

To evaluate the in vitro antiviral effect of taurultam (Fig. 1A), Vero-E6, Huh7 and 293T cell lines were used. First, the results of the CCK-8 assay revealed that taurultam did not induce apparent cytotoxicity to Vero-E6, Huh7 or 293T cells at a concentration of 30 $\mu\text{g}/\text{mL}$ or lower (Fig. 1B) and significantly improved the viability of Vero-E6 cells infected with SARS-CoV-2 and multiple variants, with EC_{50} values of 1.23 $\mu\text{g}/\text{mL}$ for the BJ01 strain, 0.68 $\mu\text{g}/\text{mL}$ for the Delta strain, 6.85 $\mu\text{g}/\text{mL}$ for the XBB 1.9.1 strain, and 13.23 $\mu\text{g}/\text{mL}$ for the BF.7 strain (Fig. 1C). At 48 hpi, the virus load in the cell supernatant was measured, and the results revealed that taurultam decreased viral RNA copy numbers in Vero-E6 (Fig. 1D) and Huh7 (Fig. 1E) cell supernatants in a dose-dependent manner. Moreover, the protein expression of the viral NP protein (Fig. 1F, G) and the viral load (Fig. 1H) in 293T-ACE2 cells were significantly decreased by taurultam at concentration of 30 $\mu\text{g}/\mu\text{L}$. These results indicated that

taurultam exhibited potent antiviral activity against different SARS-CoV-2 variants in multiple cell lines.

Taurultam protects mice and golden hamsters from nonlethal and lethal SARS-CoV-2 infection in vivo

Next, the in vivo therapeutic efficacy of taurultam against SARS-CoV-2 was assessed in BALB/c mice and golden hamsters. In a BALB/c mouse model infected with a lethal dose of SARS-CoV-2/C57MA14 (Fig. 2A), taurultam mitigated the loss of mouse body weight (Fig. 2B) and improved survival, from 14.28 to 42.86% (Fig. 2C). After taurultam was administered for five consecutive days, the mice were sacrificed, and the tissues were collected for histopathological analysis and detection of the viral load. According to gross analysis, the patchy hemorrhage observed on the lung surface of virus-infected mice was significantly reduced by taurultam (Fig. 2D), with a decrease in the lung index (Fig. 2E). Histological analysis of lung sections from each group revealed that taurultam administration apparently decreased inflammatory cell infiltration, hemorrhage, alveolar wall thickening (Fig. 2D, F) and viral NP protein expression (Fig. 2D, G).

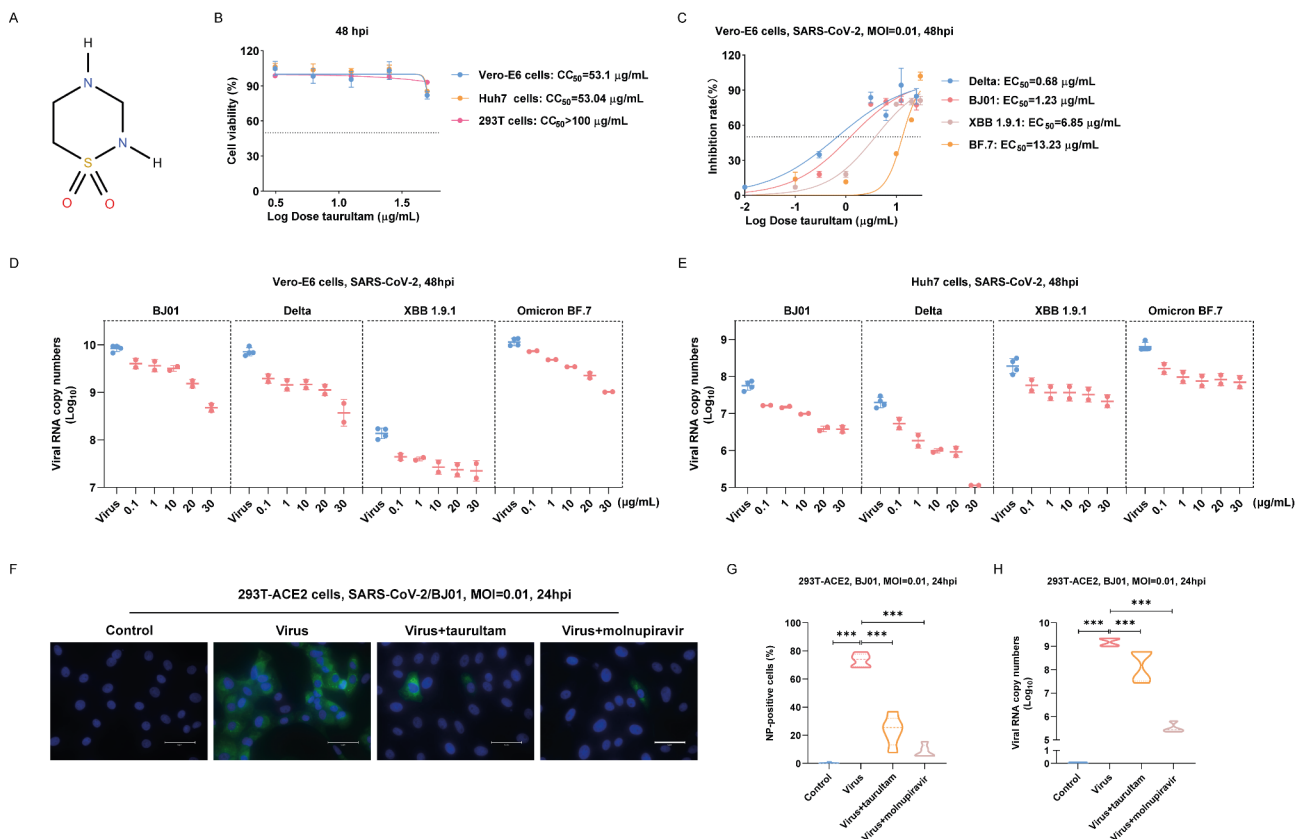


Fig. 1 Taurultam shows potent antiviral activity against different SARS-CoV-2 variants in vitro. **(A)** Chemical formula of taurultam. **(B)** Effects of taurultam on the activity of **(B)** Vero-E6, **(C)** Huh7, and **(D)** 293T cells in a series of concentrations. **(C)** The inhibitory effects of taurultam on **(E)** SARS-CoV-2/BJ01, **(F)** Delta, **(G)** XBB 1.9.1, and **(H)** BF.7 in the Vero-E6 cell line. **(D-E)** Taurultam decreased the number of viral RNA copies of SARS-CoV-2/BJ01, Delta, XBB 1.9.1, and BF.7 in the cell supernatants of the **(D)** Vero-E6 and **(E)** Huh7 cell lines. **(F-H)** The inhibitory effects of taurultam (30 $\mu\text{g}/\text{mL}$) and molnupiravir (20 $\mu\text{g}/\text{mL}$) on **(F-G)** NP protein expression and **(H)** viral RNA copy numbers of SARS-CoV-2 in the 293T-ACE2 cell line. Scale bars = 50 μm

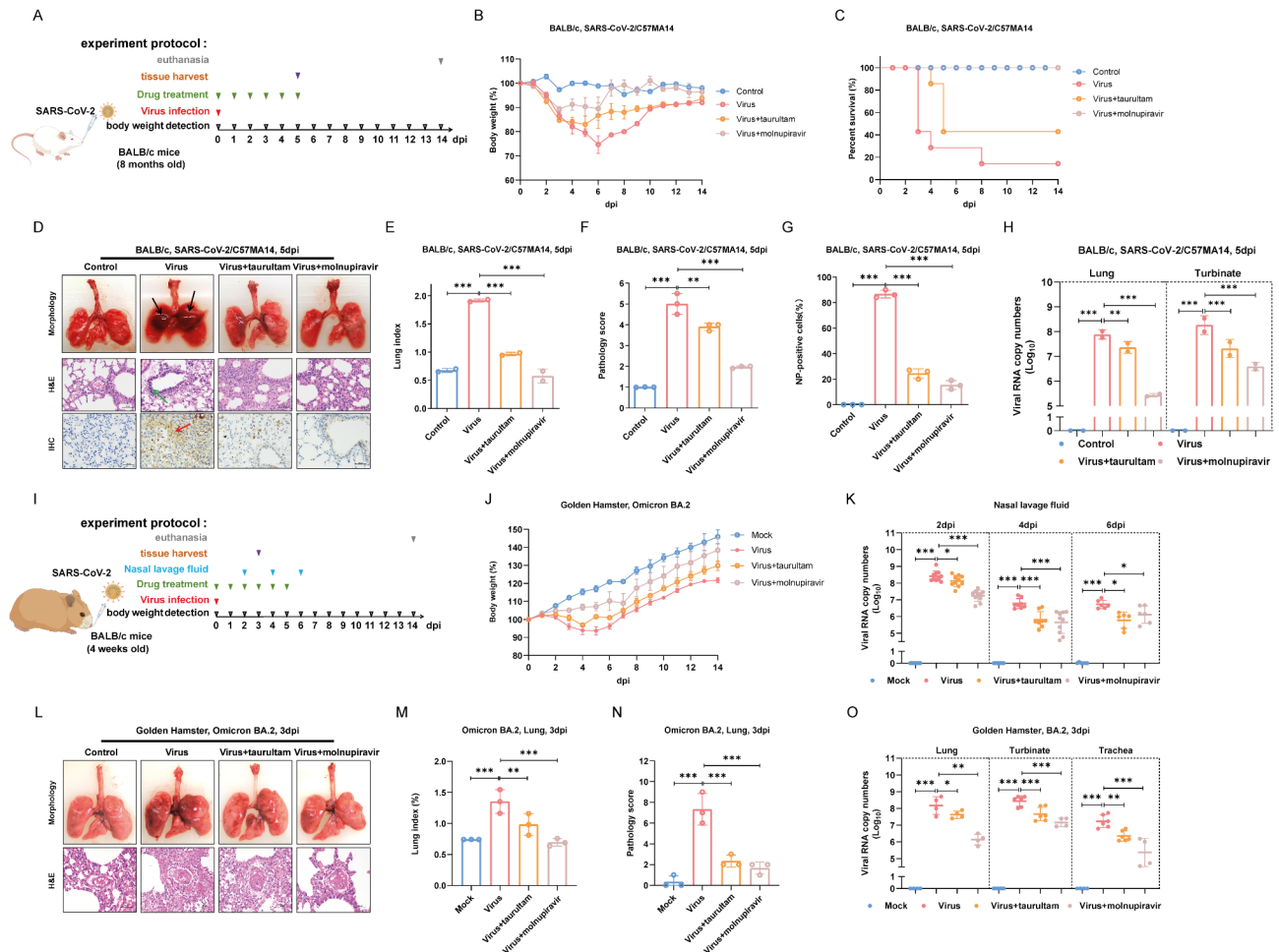


Fig. 2 Taurultam protects mice and golden hamsters from nonlethal and lethal SARS-CoV-2 infection in vivo. **(A)** Flow chart of the mouse experiment. **(B)** Effects of taurultam on the body weights of mice infected with the SARS-CoV-2/C57MA14 strain. **(C)** Taurultam improved mouse survival. **(D)** Lung tissues of the mice from each group and the respective histopathological results (HE staining) and immunohistochemical results (viral NP staining) of the lung tissue sections. **(E-G)** Lung indices, pathology scores and NP-positive cell populations of lung tissues from the mice in each group. **(H)** Viral RNA copy numbers in mouse lung tissues and turbinates. **(I)** Flow chart of the in vivo experiments involving golden hamsters. **(J)** Effects of taurultam on the body weight of golden hamsters infected with the BA.2 strain. **(K)** Viral RNA copy numbers in nasal lavage fluid samples from golden hamsters. **(L)** Lung tissues of golden hamsters from each group and respective histopathological results (HE staining) of lung tissue sections. **(M-N)** Lung indices and pathology scores of the lung tissues of golden hamsters from each group. **(O)** Viral RNA copy numbers in lung tissues, turbinates and trachea from golden hamsters

The RT-qPCR results revealed that taurultam significantly reduced viral RNA copy numbers in lung tissues and turbinates (Fig. 2H). Similar results were observed in an infection model of golden hamsters (Fig. 2I), whose prognosis was apparently improved, including promoting the recovery of body weight (Fig. 2J), ameliorating lung hemorrhage and pathological damage, and decreasing the lung index (Fig. 2L-N). Moreover, the viral loads in the nasal lavage fluid (Fig. 2K) and tissues (Fig. 2O) of golden hamsters were similarly reduced. Additional antiviral experiments on multiple Omicron variants were performed to evaluate their antiviral potential, and the results demonstrated that taurultam could reduce the lung index and viral loads in mouse lungs and turbinates in BALB/c and C57BL/6 N model mice infected with BA.2 (Fig. 3A-C), BE.7 (Fig. 3D-F, G-I) or XBB 1.9.1

(Fig. 3J-L). Together, these results suggested that taurultam treatment inhibited SARS-CoV-2 infection and lung pathology.

Taurultam inhibits influenza A virus and influenza B virus in vitro and in vivo

Given that taurolidine is used as a potent antiviral candidate for influenza virus, it was necessary to determine the inhibitory effect of taurultam on influenza viruses. First, in vitro experiments were performed in the MDCK cell line. The results revealed that taurultam significantly inhibited the viral NP expression of influenza A virus (Fig. 4A, B) and influenza B virus (Fig. 4C, D) and the virus titre in the cell supernatant (Fig. 4E). In addition, the formation of virus-induced plaques was suppressed by taurultam (Fig. 4F, G). For in vivo antiviral

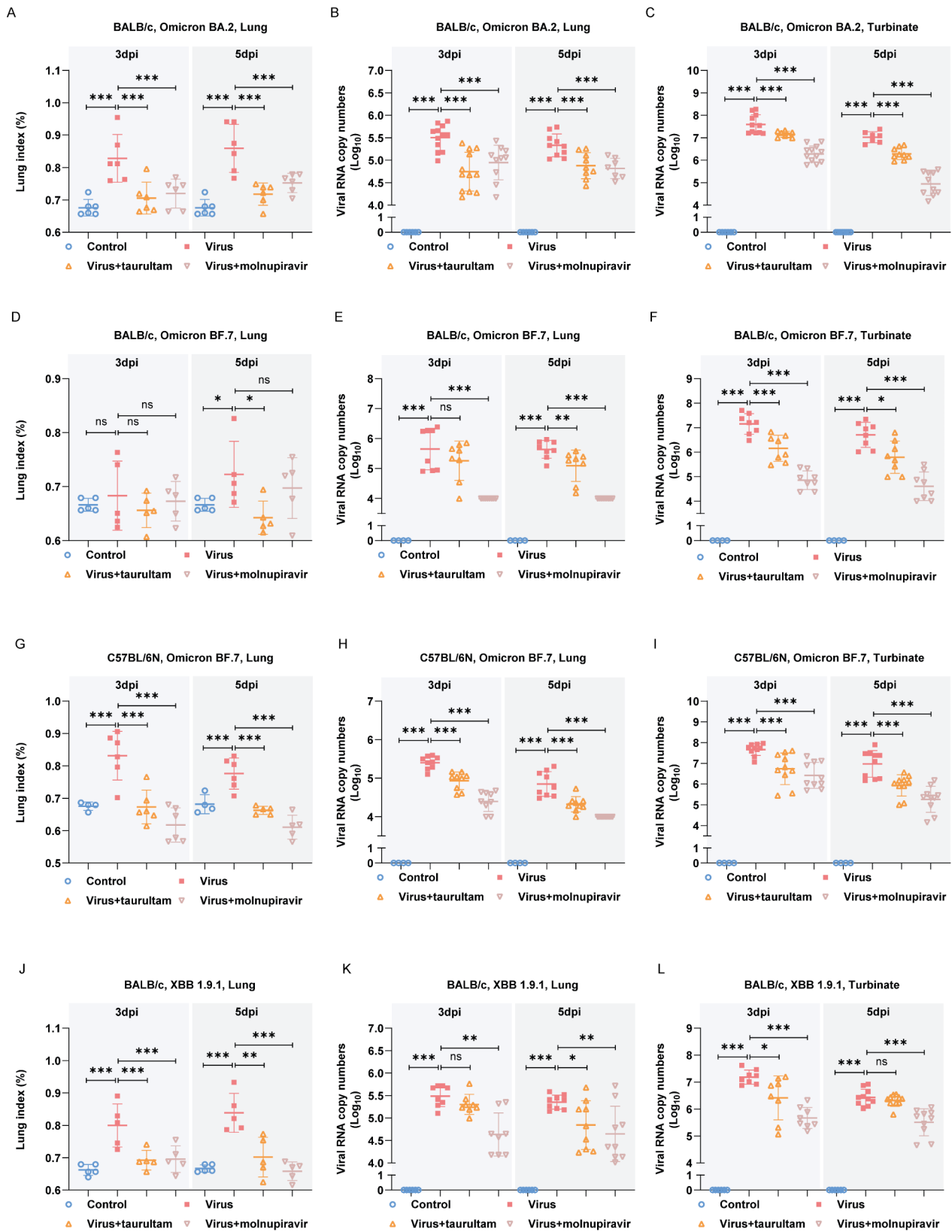


Fig. 3 Taurultam resists multiple Omicron variant infections in mouse models. (A-C) Lung indices and viral RNA copy numbers in the lung tissues and turbinates of BALB/c mice infected with Omicron BA.2. (D-F) Lung indices and viral RNA copy numbers in the lung tissues and turbinates of BALB/c mice infected with Omicron BF.7. (G-I) Lung indices and viral RNA copy numbers in the lung tissues and turbinates of C57BL/6 N mice infected with Omicron BF.7. (J-L) Lung indices and viral RNA copy numbers in the lung tissues and turbinates of BALB/c mice infected with XBB 1.9.1

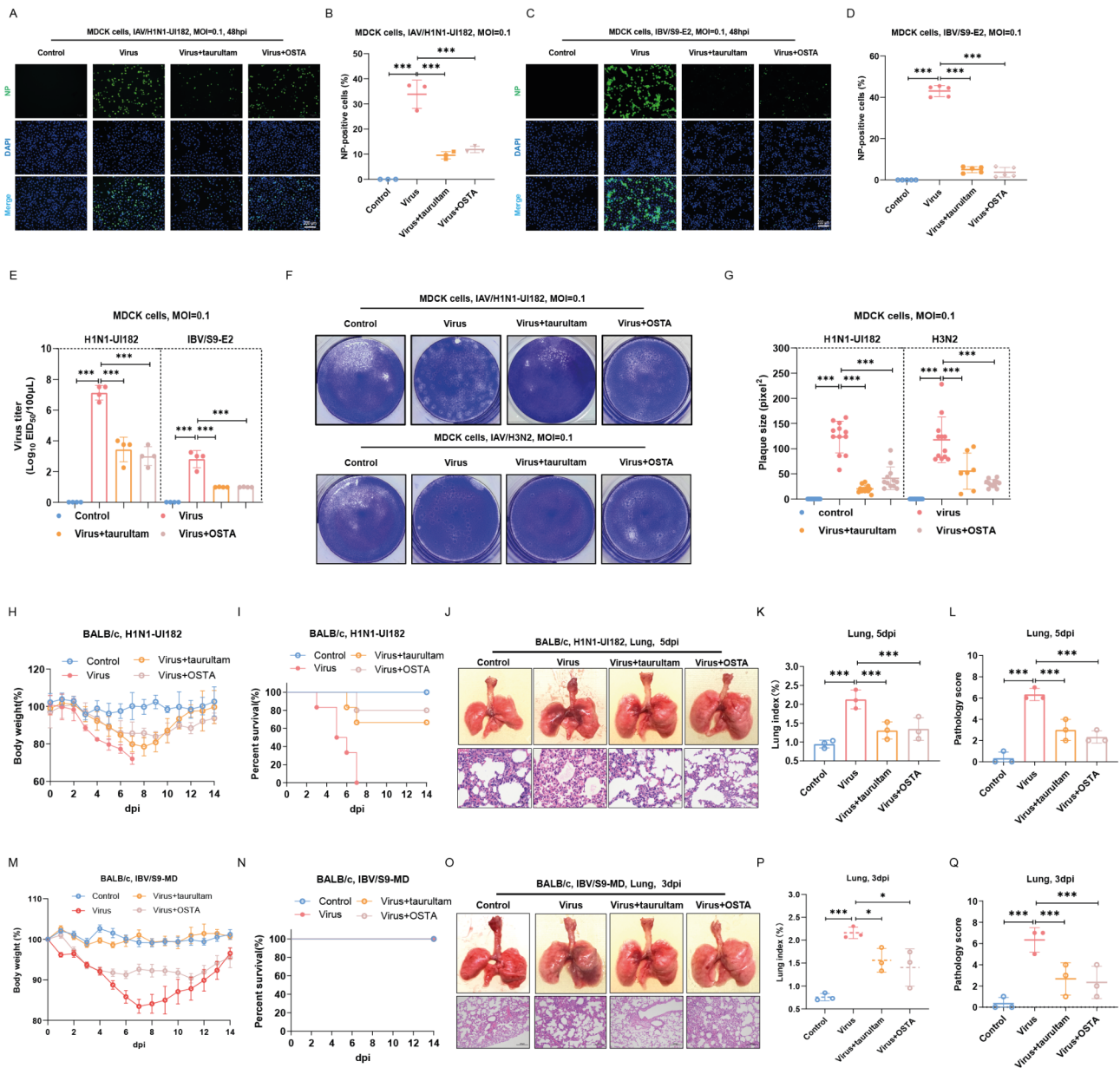


Fig. 4 Taurultam inhibits influenza A virus and influenza B virus in vitro and in vivo. **(A–D)** Effects of Taurultam on the viral NP protein expression of **(A, B)** H1N1-UI182 and **(C, D)** IBV/S9-E2 in the MDCK cell line. Scale bars = 200 μm **(E)** Effects of Taurultam on the virus titres of H1N1-UI182 and IBV/S9-E2 in MDCK cell supernatants. **(F)** Effects of taurultam on the formation of plaques induced by H1N1-UI182 and IAV/H3N2. **(G)** Sizes of plaques from three biological replicates were measured in ImageJ software. For in vitro experiment, taurultam was used at 30 $\mu\text{g}/\text{mL}$ and oseltamivir acid was used at 100 μM **(H–I)** Effects of taurultam on the **(H)** body weight and **(I)** survival rate of H1N1-UI182 strain-infected mice. **(J)** Lung tissues of mice from each group infected with H1N1-UI182 and the respective histopathological results (HE staining) of lung tissue sections. **(K–L)** Lung indices and pathology scores of lung tissues from H1N1-UI182-infected mice in each group. **(M–N)** Effects of taurultam on the **(M)** body weight and **(N)** survival rate of mice infected with the IBV/S9-MD strain. **(O)** Lung tissues of mice from each group infected with IBV/S9-MD and the respective histopathological results (HE staining) of lung tissue sections. **(P–Q)** Lung indices and pathology scores of lung tissues from mice in each group infected with IBV/S9-MD

efficacy, BALB/c mice were challenged with a lethal dose of H1N1-UI182 and a nonlethal dose of IBV/S9-MD, and then drugs were initially administered to the mice at 12 h post infection. Body weight data and survival data indicated that taurultam mitigated weight loss in both models (Fig. 4H, M) and improved mouse survival in the H1N1-UI182 infection model (Fig. 4I). At 3 dpi or 5

dpi, the mice were sacrificed, and lung tissues were collected for examination of lung histopathology. In both models, virus infection caused severe hemorrhages on the lung surface (Fig. 4J, O) and apparent elevations in the lung index (Fig. 4K, P); these symptoms were significantly relieved by taurultam treatment. HE staining of lung tissues also revealed similar results: the pathological

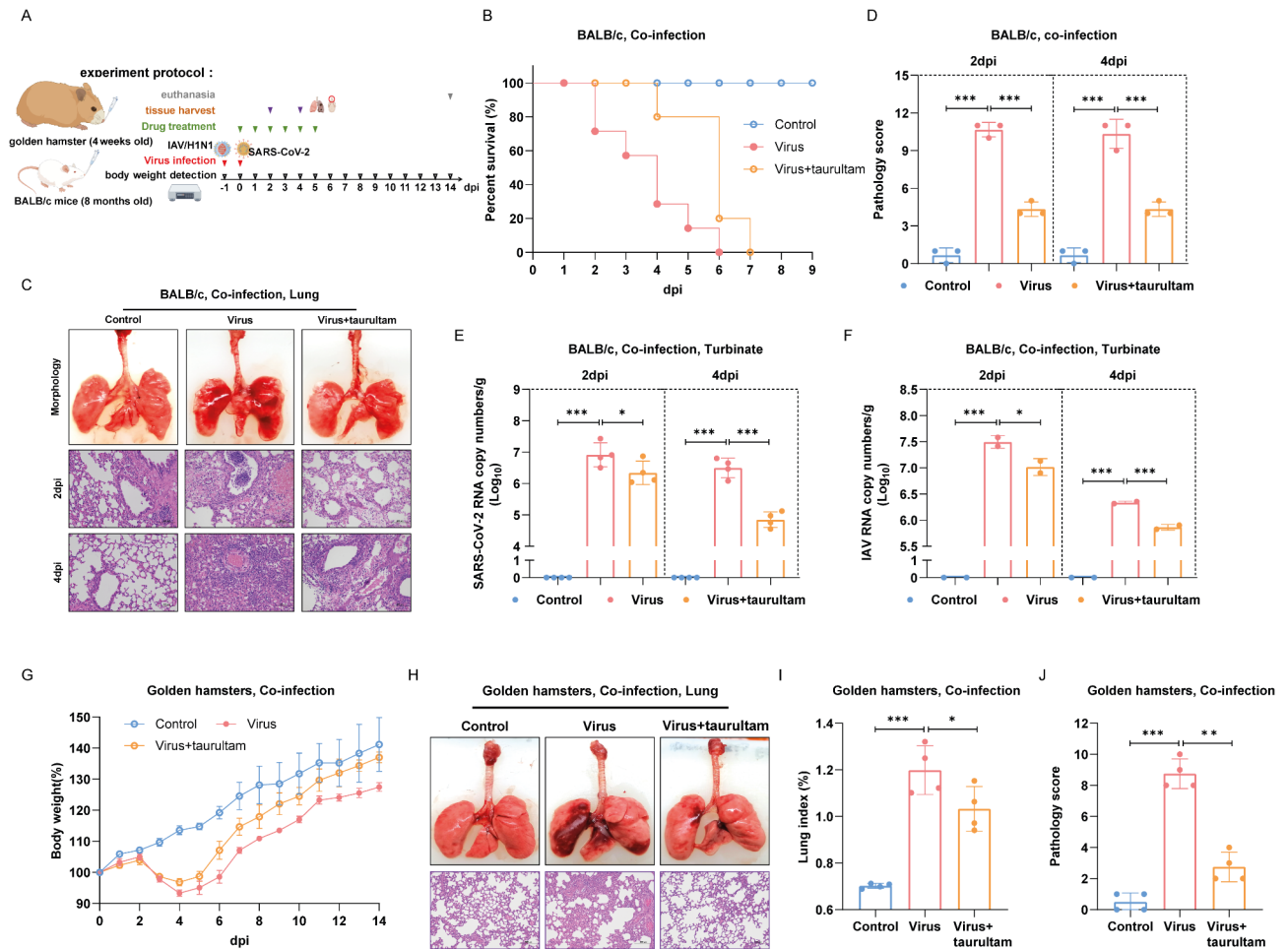


Fig. 5 Taurultam benefit for the treatment of coinfection with influenza A virus and SARS-CoV-2. **(A)** Flow chart of the coinfection experiment. **(B)** Effect of taurultam on the survival rate of BALB/c mice coinfecting with H1N1-UI182 and SARS-CoV-2/C57MA14. **(C)** Lung tissues of mice from each group infected with H1N1-UI182 and the respective histopathological results (HE staining) of lung tissue sections at 2 dpi and 4 dpi. **(D)** Pathology scores of the lung tissues of the mice in each group. **(E-F)** Effects of taurultam on the viral loads of SARS-CoV-2 and H1N1 in mouse turbinates at 2 dpi and 4 dpi. **(G)** Effects of taurultam on the body weight of golden hamsters coinfecting with H1N1-UI182 and Omicron BF.7. **(H)** Lung tissues of golden hamsters and histopathological results (HE staining) of lung tissue sections at 3 dpi. **(I-J)** Lung indices and pathology scores of lung tissues from golden hamsters in each group

damage to the lungs of taurultam-treated mice was apparently milder than that to the lungs of virus-infected mice (Fig. 4J, O), as were the lung pathology scores (Fig. 4L, Q). These results indicate that taurultam has potent antiviral effects on both influenza A virus and influenza B virus.

Taurultam benefits for therapy of coinfection of influenza A virus and SARS-CoV-2

The above results demonstrated that taurultam strongly inhibited both influenza virus and SARS-CoV-2, and we then assessed whether taurultam has therapeutic effects on mixed infections with these two viruses. BALB/c mice and golden hamsters were challenged with H1N1-UI182 and SARS-CoV-2, respectively, and taurultam treatment was initiated 12 h after SARS-CoV-2 infection for 5 days (Fig. 5A). In the BALB/c mouse model, taurultam

treatment delayed the death of infected mice (Fig. 5B), improved pathological damage to the lungs (Fig. 5C, D) and decreased the viral loads of H1N1-UI182 (Fig. 5F) and SARS-CoV-2 (Fig. 5E) in lung tissues. Meanwhile, the viral NP protein expressions of two viruses were reduced by taurultam at 2 dpi and 4 dpi (Fig. S1). Similar results were obtained in golden hamsters, and the reductions in mouse body weight (Fig. 5H), pulmonary hemorrhage (Fig. 5I) and lung pathological damage (Fig. 5I-K) were mitigated by taurultam treatment. Overall, taurultam treatment not only suppressed the influenza A virus and SARS-CoV-2 alone, but also improved the effectiveness of mixed infection with these two viruses.

Discussion

SARS-CoV-2 and influenza virus, which are highly infective and pathogenic, are two respiratory viruses that pose major threats to human and public health [12, 13]. Owing to their high mutational frequency, novel variants with drug resistance challenge the available antiviral agents and prompt the urgent need for the development of new therapeutics. Additionally, mixed infections caused by diverse respiratory pathogens create a clinical conundrum of drug combination strategies. Thus, the development of broad-spectrum antivirals against multiple respiratory viruses is important. In this study, taurultam exhibited potent broad-spectrum antiviral activities against SARS-CoV-2 and influenza virus in both in vitro and in vivo models. In particular, taurultam exhibited significant therapeutic efficacy in mixed infection models, indicating good potential for antiviral therapy. However, its clinical application prospects need further preclinical and clinical research for validation.

Taurolidine is an outstanding and safe antimicrobial, antiadhesion, antioxidant and anti-inflammatory agent without significant toxic side effects. Owing to its high hydrolysis capacity and kinetics, the biological functions of taurolidine are determined by its metabolites, namely, taurultam, N-methyltaurultam, N-methyltaurultamide and taurine [14]. For example, taurolidine breaks bacterial cell walls [15–17] through chemical cross-linking of its N-methylol metabolites and proteins in the bacterial cell wall, and its antioxidant and anti-inflammatory functions are performed by the end product taurine [18, 19]. In this study, we first demonstrated that taurultam exhibited potent antiviral activity against SARS-CoV-2 and influenza virus, similar to taurolidine, indirectly suggesting that taurultam plays a vital role in the antiviral response to taurolidine. And a comparative study was carried out in our experiments, the results showed that the antiviral effect of taurolidine was similar to that of taurultam, both of them significantly reduced the viral load in the hamster tissues (Fig. S2C-F), but the effect of taurolidine on improvement of lung injury is significantly better than that of taurultam (Fig. S2A, B). From these data, we can speculate that taurultam may be the main ingredient that accounts for antiviral of taurolidine, and of course, there is a possibility that taurolidine and taurultam both exert antiviral activity through the same antiviral pathways. Since the antiviral mechanism of taurolidine has not been fully resolved, more research is also needed on antiviral mechanisms of taurultam. In addition, a previous study showed that taurolidine inhibited severe lung injury induced by influenza A (H5N1) virus infection through inhibiting NF- κ B signaling pathway [9], and the metabolite taurultam also significantly ameliorated viral lung injury, suggesting that taurultam may

also inhibit lung inflammation through inhibiting NF- κ B signaling pathway.

Lung damage is the first manifestation of multiple organ dysfunction syndrome caused by SARS-CoV-2 and influenza virus and is induced mainly by viral infection of epithelial cells and cytokine storm syndrome. Indeed, treatment during the acute infection phase of COVID-19 and flu may influence the degree of clinical manifestations of “long COVID” and “long flu”; timely removal of viruses and attenuation of lung tissue injury may thus result in better outcomes [20]. Taurultam was found to accelerate virus clearance and improve virus-induced lung damage, suggesting that it may become a potential candidate for treating COVID-19 and flu at the early stage of infection. Given the outstanding ability of taurultam to alleviate lung injury, the anti-inflammatory function of its metabolic end product taurine [21–24] may partially explain this association.

Conclusion

In this study, we identified an antiviral candidate, taurultam, that exhibited significant antiviral effects on SARS-CoV-2 and influenza viruses both in vitro and in vivo. Taurultam not only decreased viral loads in mouse models but also significantly alleviated lung pathological damage caused by both SARS-CoV-2 and influenza viruses. Additionally, as a metabolite of taurolidine whose biological functions are always performed by its metabolites, the antiviral activities of taurultam are similar to those of taurolidine, suggesting that taurultam may be partly responsible for the antiviral response of taurolidine. These findings provide solid experimental evidence for the clinical application of taurultam and taurolidine.

Abbreviations

PBS	Phosphate buffered saline
DMEM	Dulbecco's Modified Eagle's Medium
OSTA	Oseltamivir
MOI	Multiplicities of infection
hpi	Hour post infection
dpi	Day post infection
CC ₅₀	Cytotoxic concentration for 50% of cells
EC ₅₀	Half-maximal effective concentration
RT	Room temperature
i.p.	Intraperitoneal injection
p.o.	Oral administration
COVID-19	Corona virus disease 2019

Supplementary Information

The online version contains supplementary material available at <https://doi.org/10.1186/s12866-025-03847-2>.

Supplementary Material 1

Acknowledgements

Null.

Author contributions

Yuwei Gao, Wu Zhong and Xiaobin Pang designed experiments and provided guidance. SARS-CoV-2 infection experiments were performed by Rongbo Luo, Beilei Shen, Bingshuo Qian, Lingjun Fan, and Junkui Zhang. Influenza virus infection experiments were performed by Rongbo Luo, Bingshuo Qian, Chaoliang Lv, Xiuwen Deng, Yan Sun and Shijun Zhang. All viruses used in this research were provided by Yuanguo Li, Weiyang Sun and Tiecheng Wang.

Funding

This work was supported by the National Key Research and Development Program of China (2023YFC0871000 and 2023YFF1305400).

Data availability

Data is provided within the manuscript. The data produced from this study are available from the first author and the corresponding authors on reasonable request.

Declarations

Animal ethics approval and biosafety statement

Animal experiments were conducted following the protocols of the Changchun Veterinary Research Institute, Chinese Academy of Agricultural Sciences (approval number: IACUC of AMMS-11-2022-036). The mice were anaesthetized via inhalation of 2.0% isoflurane, infected with nasal viral drops, and then naturally awakened. The endpoint of observation was defined as either natural death or a weight less than 75% of the original weight. The mice were euthanized once their weight was lower than 75% of the initial body weight via the inhalant euthanasia agent carbon dioxide. Additionally, all influenza virus infection experiments were conducted in a biosafety level 2 laboratory, and all SARS-CoV-2 infection experiments were conducted in a biosafety level 3 laboratory according to biosafety regulations.

Consent for publication

Not applicable.

Competing interests

The authors declare no competing interests.

Received: 21 November 2024 / Accepted: 25 February 2025

Published online: 15 May 2025

References

1. Dhama K, et al. Global emerging Omicron variant of SARS-CoV-2: impacts, challenges and strategies. *J Infect Public Health*. 2023;16(1):4–14.
2. Kinoshita T, et al. Co-infection of SARS-CoV-2 and influenza virus causes more severe and prolonged pneumonia in hamsters. *Sci Rep*. 2021;11(1):21259.
3. Bai L, et al. Coinfection with influenza A virus enhances SARS-CoV-2 infectivity. *Cell Res*. 2021;31(4):395–403.
4. Zhang W, et al. Frequency and distribution of H1N1 influenza A viruses with oseltamivir-resistant mutations worldwide before and after the 2009 pandemic. *J Med Virol*. 2022;94(9):4406–16.
5. Chromik AM, et al. Comparative analysis of cell death induction by taurolidine in different malignant human cancer cell lines. *J Exp Clin Cancer Res*. 2010;29(1):21.
6. Koldehoff M, Zakrzewski JL. Taurolidine is effective in the treatment of central venous catheter-related bloodstream infections in cancer patients. *Int J Antimicrob Agents*. 2004;24(5):491–5.
7. Baker DM, et al. Taurolidine peritoneal lavage as prophylaxis against infection after elective colorectal surgery. *Br J Surg*. 1994;81(7):1054–6.
8. Simon A, et al. Taurolidine-citrate lock solution (TauroLock) significantly reduces CVAD-associated grampositive infections in pediatric cancer patients. *BMC Infect Dis*. 2008;8:102.
9. Lv C, et al. Taurolidine improved protection against highly pathogenic avian influenza H5N1 virus lethal-infection in mouse model by regulating the NF-kappaB signaling pathway. *Virology*. 2023;38(1):119–27.
10. Gong L, et al. The pharmacokinetics of taurolidine metabolites in healthy volunteers. *J Clin Pharmacol*. 2007;47(6):697–703.
11. Luo R, et al. A potential Chinese medicine monomer against influenza A virus and influenza B virus: isoquercitrin. *Chin Med*. 2023;18(1):144.
12. Uyeki TM, Hui DS, Zambon M, Wentworth DE, Monto AS. Influenza Lancet. 2022;400(10353):693–706.
13. Silva S, et al. Recent insights into SARS-CoV-2 Omicron variant. *Rev Med Virol*. 2023;33(1):e2373.
14. Stendel R, et al. Pharmacokinetics of taurolidine following repeated intravenous infusions measured by HPLC-ESI-MS/MS of the derivatives taurultame and taurinamide in glioblastoma patients. *Clin Pharmacokinet*. 2007;46(6):513–24.
15. Marley K, et al. Pharmacokinetic study and evaluation of the safety of taurolidine for dogs with osteosarcoma. *J Exp Clin Cancer Res*. 2013;32(1):74.
16. Giaccardi M et al. Salvage of cardiac implantable electronic device pocket infection with skin erosion in frail 92-Year-Old. *J Cardiovasc Dev Dis*, 2022. 9(3).
17. Neary PM, et al. The evolving role of taurolidine in cancer therapy. *Ann Surg Oncol*. 2010;17(4):1135–43.
18. Ashkani-Esfahani S, et al. Taurine improves the wound healing process in cutaneous leishmaniasis in mice model, based on Stereological parameters. *Adv Biomed Res*. 2014;3:204.
19. Watson RW, et al. Taurolidine, an antilipopolysaccharide agent, has immunoregulatory properties that are mediated by the amino acid taurine. *J Leukoc Biol*. 1995;58(3):299–306.
20. Fung KW, et al. Prevalence and characteristics of long COVID in elderly patients: an observational cohort study of over 2 million adults in the US. *PLoS Med*. 2023;20(4):e1004194.
21. Bhavsar TM, et al. Attenuating effect of taurine on lipopolysaccharide-induced acute lung injury in hamsters. *Pharmacol Res*. 2009;60(5):418–28.
22. Coffey MJ, et al. Gut microbiota in children with cystic fibrosis: A taxonomic and functional dysbiosis. *Sci Rep*. 2019;9(1):18593.
23. Bao X, et al. Roles of dietary amino acids and their metabolites in pathogenesis of inflammatory bowel disease. *Mediators Inflamm*. 2017;2017:p6869259.
24. Qaradakhi T et al. The Anti-Inflammatory effect of taurine on cardiovascular disease. *Nutrients*, 2020. 12(9).

Publisher's note

Springer Nature remains neutral with regard to jurisdictional claims in published maps and institutional affiliations.